The Astrophysical Journal Letters, 946:L29 (6pp), 2023 March 20 https://doi.org/10.3847/2041-8213/acc247
© 2023. The Author(s). Published by the American Astronomical Society.
OPEN ACCESS

Observation of Anomalous Electron Fluxes Induced by GRB221009A on CSES-01 Low-energy Charged Particle Detector

R. Battiston[1], C. Neubüser[2], F. M. Follega[1,2], R. Iuppa[1], V. Vitale[3], R. Ammendola[4], D. Badoni[4], S. Bartocci[4], A. Bazzano[5], S. Beolè[6], I. Bertello[5], W. J. Burger[2], D. Campana[7], A. Cicone[8], P. Cipollone[4], S. Coli[9], L. Conti[4,10], A. Contin[11], M. Cristoforetti[12], G. D'Angelo[5], F. De Angelis[5], C. De Donato[4], C. De Santis[4], P. Diego[5], A. Di Luca[1], E. Fiorenza[5], G. Gebbia[1,2], A. Lega[1,2], M. Lolli[13], B. Martino[14], M. Martucci[4], G. Masciantonio[4], M. Mergè[15], M. Mese[7,16], A. Morbidini[5], F. Nuccilli[5], F. Nozzoli[2], A. Oliva[11], G. Osteria[7], E. Papini[5], F. Palma[4], F. Palmonari[11], A. Parmentier[5], B. Panico[7,16], S. Perciballi[6], F. Perfetto[7], A. Perinelli[1], P. Picozza[3], M. Piersanti[8], M. Pozzato[13], G. Rebustini[4], D. Recchiuti[5], E. Ricci[1,2], M. Ricci[17], J. Rodi[5], A. Russi[5], S. B. Ricciarini[18], Z. Sahnoun[11,13], U. Savino[6], V. Scotti[7,16], X. Shen[19], A. Sotgiu[4], R. Sparvoli[3], S. Tofani[5], P. Ubertini[5], N. Vertolli[5], V. Vilona[2], U. Zannoni[5], Z. Zeren[20], S. Zoffoli[15], and P. Zuccon[1]
[1] University of Trento, Via Sommarive 14, I-38123 Trento, Italy
[2] TIFPA-INFN, Via Sommarive 14, I-38123 Trento, Italy; coralie.neubueser@tifpa.infn.it
[3] University of Rome, Tor Vergata, I-38123 Rome, Italy
[4] INFN—Sezione di Roma Tor Vergata, Via della Ricerca Scientifica 1, I-00133, Rome, Italy
[5] INAF-IAPS, Via Fosso del Cavaliere 100, I-00133, Rome, Italy
[6] Università di Torino, Via P. Giuria 1, I-10125 Torino, Italy
[7] INFN—Sezione di Napoli, Via Cintia, I-80126, Naples, Italy
[8] University of L'Aquila, Via Vetoio, I-67100, L'Aquila, Italy
[9] INFN—Sezione di Torino, Via P. Giuria 1, I-10125 Torino, Italy
[10] Uninettuno University, C.so Via Emanuele II, 39, I-00186, Rome, Italy
[11] Università di Bologna, Viale Berti Pichat 6/2, I-40127 Bologna, Italy
[12] Fondazione Bruno Kessler, Via Sommarive 18, I-38123 Povo, Italy
[13] INFN—Sezione di Bologna, Viale Berti Pichat 6/2, I-40127 Bologna, Italy
[14] CNR, Via Fosso del Cavaliere 100, I-00133, Rome, Italy
[15] Italian Space Agency, Via del Politecnico, I-00133 Rome, Italy
[16] Università degli Studi di Napoli Federico II, Via Cintia, I-80126, Naples, Italy
[17] INFN—LNF, Via E. Fermi, 54, I-00044 Frascati (RM), Italy
[18] IFAC-CNR, Via Madonna del Piano, 10, I-50019 Sesto Fiorentino (FI), Italy
[19] National Space Science Center, Chinese Academy of Sciences, Beijing 100190, People's Republic of China
[20] National Institute of Natural Hazards, Ministry of Emergency Management of China, Beijing 100085, People's Republic of China
Received 2023 February 17; revised 2023 March 7; accepted 2023 March 8; published 2023 March 28

Abstract

High-energy, long gamma-ray bursts (GRBs) can be generated by the core collapse of massive stars at the end of their lives. When they happen in the close-by universe they can be exceptionally bright, as seen from the Earth in the case of the recent, giant, long-lasting GRB221009A. GRB221009A was produced by a collapsing star with a redshift of 0.152: this event was observed by many gamma-ray space experiments, which also detected an extraordinary long gamma-ray afterglow. The exceptionally large fluence of the prompt emission of about 0.013 erg cm^{-2} illuminated a large geographical region centered on India and including Europe and Asia. We report in this paper the observation of sudden electron flux changes correlated with GRB221009A and measured by the HEPP-L charged particle detector on board the China Seismo-Electromagnetic Satellite, which was orbiting over Europe at the time of the GRB event. The time structure of the observed electron flux closely matches the very distinctive time dependence of the photon flux associated with the main part of the emission at around 13:20 UTC on 2022 October 9. To test the origin of these signals, we set up a simplified simulation of one HEPP-L subdetector: the results of this analysis suggest that the signals observed are mostly due to electrons created within the aluminum collimator surrounding the silicon detector, providing real-time monitoring of the very intense photon fluxes. We discuss the implications of this observation for existing and forthcoming particle detectors on low Earth orbits.

Unified Astronomy Thesaurus concepts: Particle astrophysics (96); Gamma-ray bursts (629); Astronomical detectors (84)

1. Introduction

Gamma-ray bursts (GRBs) are generated by highly energetic astrophysical events, producing intense bursts of photons reaching Earth after a long journey in space. For their neutral nature and low cross section to intergalactic matter, they travel without being perturbed by magnetic fields and, as a result, the universe is quite transparent to their passage up to very high redshift. The measurement of the characteristics of these events (time structure and energy spectrum) has been key to understand the nature of their progenitors and to model the relativistic emission processes generating the most energetic phenomena present in the universe. Thus, these data play an important role in observational astrophysics, by providing a

Original content from this work may be used under the terms of the Creative Commons Attribution 4.0 licence. Any further distribution of this work must maintain attribution to the author(s) and the title of the work, journal citation and DOI.

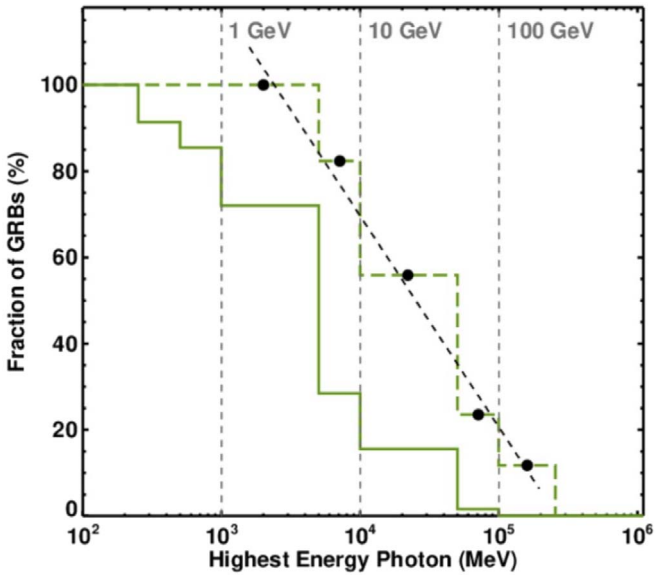

Figure 1. Fraction of GRBs with the highest-energy photon detected by Fermi above selected threshold energies (Ajello et al. 2019). The energy distribution corrected for the source redshift is indicated by the dashed green line. The dashed black line shows a linear fit to the values corresponding to the center of each bin.

unique tool for the study of the evolution and its chemical composition. Long-lasting GRBs are rare events, and the brightest, in terms of flux measurable on Earth, occur only every few years. Their maximum flux is usually in the MeV range, and at higher energies the probability of detecting a GRB photon decreases exponentially, as shown in Figure 1.

On 2022 October 9, at 13:16:59 UTC, telescopes on board Earth-orbiting satellites detected the brightest long gamma-ray burst ever recorded in the history of observational astrophysics. GRB221009A was located at R.A. $= +19^{h}\ 14^{m}\ 03^{s}$ and decl. $= +19^{d}50'33''$, which corresponds to a zenith over India, at about $+71^{\circ}$ longitude and $+19^{\circ}.8$ latitude. The GRB illuminated most of Europe, Asia, Africa, and Australia. The highest photon energy reported in association with this GRB has been measured at 18 TeV by the LHAASO (Huang et al. 2022) ground array experiment in China.

The GRB triggered several space-based instruments sensitive to gamma rays, such as Swift with the Burst Alert Telescope (BAT; Dichiara et al. 2022), Fermi with the Gamma-ray Burst Monitor (GBM; Lesage et al. 2022) and INTEGRAL (Götz et al. 2022) with its Burst Alert System (IBAS; Mereghetti et al. 2003).

Measurements have also been performed by the Spectrometer/Telescope for Imaging X-rays (STIX) on Solar Orbiter (Xiao et al. 2022), the Pixellated Imaging CsI Telescope (PICsIT) and the anti-coincidence shield of the pectrometer (SPI/ACS) on INTEGRAL (Götz et al. 2022), and the High Energy Burst Searcher (HEBS) on SATech-01 (Liu et al. 2022a).

The main component of GRB221009A was so intense, that most gamma-ray burst monitors showed signs of saturation during the main GRB emission, between 13:20:40 and 13:21:30 UTC. HEBS, however, followed the main part of gamma flux evolution without data saturation and subsecond timing resolution: for this reason we will use HEBS data (Liu et al. 2022b) in this work.

Extremely bright GRBs produce a strong ionization in Earth's top atmospheric layers. A fraction of the electrons produced during the ionization may, after diffusion, be trapped in the Earth's magnetic field and detected by space borne low-energy charged particle detectors. However, considering the extraordinary brightness of GRB221009A, other processes could also be present, like the direct interaction of energetic photons with the particle detectors structure, producing low-energy, secondary electrons. For these reasons we investigated the response to this GRB of HEPP-L, the sensitive low-energy particle detector on board the low Earth orbit (LEO) China Seismo-Electromagnetic Satellite (CSES-01; Shen et al. 2018).

2. The HEPP-L Detector on board the CSES-01 Satellite

The CSES mission is a joint collaboration between the China National Space Administration (CNSA) and the Italian Space Agency (ASI). The CSES-01 satellite is a state-of-the-art multipayload space observatory, launched in 2018 February. It is orbiting around the Earth at an altitude of about 500 km on a Sun-synchronous orbit circling the Earth 16 times a day, with a revisiting time of 5 days. The scientific objectives of the missions are as follows: investigation of the Van Allen Belts dynamics, gathering data on particle and plasma perturbations caused by geophysical and other natural sources as well as anthropic emitters; the study of solar-terrestrial interactions and impulsive phenomena from the Sun, like coronal mass ejections, solar energetic particles, and solar flares; the extension of cosmic-ray measurements of low-energy protons and electrons, from 100 keV to hundreds of MeV.

CSES-01 carries a suite of nine instruments operating in a latitude region between $\pm 65^{\circ}$. In particular, it is equipped with payloads measuring charged particles on a wide range of energies. Among the particle detectors there is the High-energy Particle Package (HEPP; Li et al. 2019) which is composed by three detectors: HEPP-L, HEPP-H, and HEPP-X. The first two are designed to measure low-energy (0.1–55 MeV) and high-energy (2–230 MeV) charged particles respectively and are mostly sensitive to electrons and protons trapped in the Van Allen Belts. The last one is built to monitor the solar gamma-ray component up to tens of keV.

The HEPP-L detector is shown in Figure 2. It is composed of two main subsystems: a silicon detector, consisting of a thin and thick silicon layer and an anticoincidence detector made of plastic scintillator.

The nine silicon detectors with their cylindrical aluminum collimators and fanned out orientation allow for the measurement of the particle direction over a wide range of angles. The particle identification is based on the dE/dx measurement between the silicon layers, which results in an estimated proton contamination in the electron sample below 10% for L-shell values below 4 (Zhang et al. 2022). A more detailed description of the HEPP-L detector can be found in (Li et al. 2019).

3. Methods

The data of all instruments on board CSES-01 are regularly uploaded and made available on https://leos.ac.cn. The electron flux data of HEPP-L are provided as high-level calibrated data, which include the conversion of electron rates to fluxes. Such fluxes are measured every second by each silicon unit separately, and are divided in 256 energy bins, each covering a range of 11 keV, spanning an energy range from

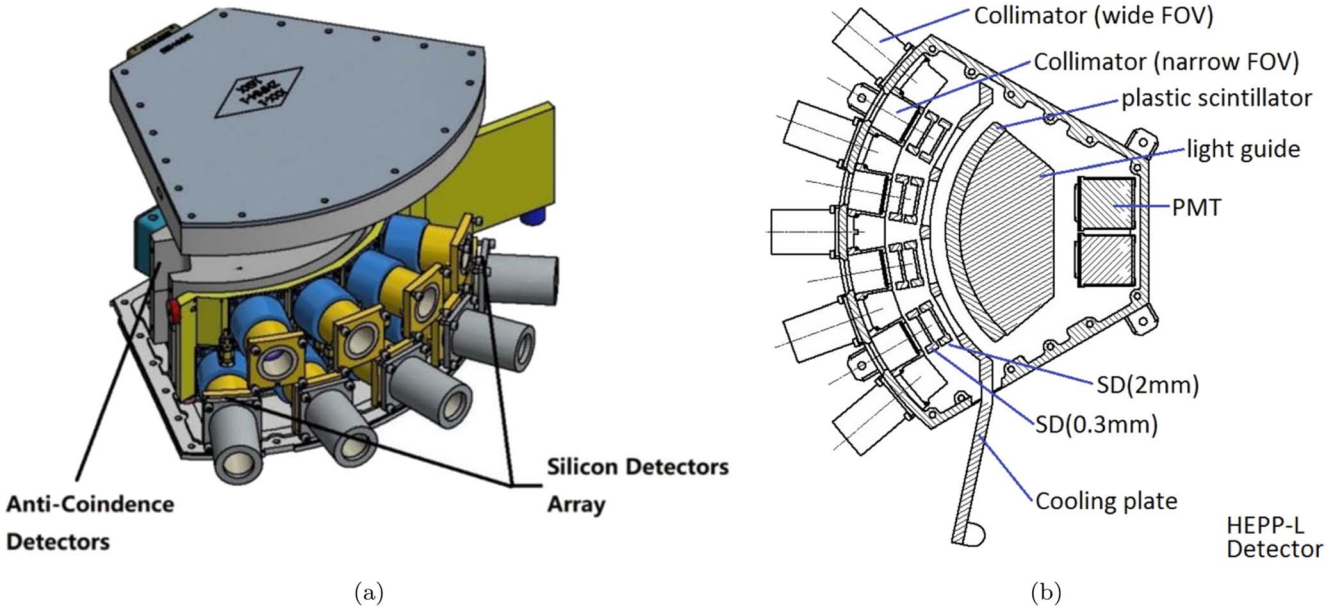

Figure 2. A Computer-Aided Design (CAD) rendering and a schematic top view of HEPP-L are show in (a) and (b), respectively. The collimator system, the anticoincidence detector (plastic scintillator), used to shield from out-of-acceptance particles, and the silicon detector (SD) are displayed in (b) (Li et al. 2019).

100 keV up to 3 MeV. The telemetry provides the satellite position (longitude, latitude, altitude, and L-shell) and UTC time. The L shell is a parameter that refers to the crossed magnetic field lines defined by their height in Earth radii at the magnetic equator. Its value, also known as the McIlwain parameter (McIlwain 1961), is a key parameter in describing the trapped particle populations of the Van Allen radiation belts.

3.1. Identification of Anomalous Signals

In order to identify anomalous signals, we used a method that compares the actual measurement with a corresponding baseline computed for different regions of the L-shell/equatorial pitch angle α_{eq} invariant phase space. A detailed description of the method can be found in Neubüser et al. (2023). The division in L/α_{eq} cells is optimized for maximum sensitivity in the low L-shell regions and adapted to the angular resolution of the detector. In order to reduce computational time necessary for the extraction of the background estimates and for the clustering into particle bursts (PBs), the HEPP-L fluxes are consolidated in 11 out of the 256 original energy bins. For every energy bin and L/α_{eq} cell having a minimum 50 entries per day, the background estimation provides an average flux value, μ, and a standard deviation, σ. Then, we set a threshold of $\mu + 3\sigma$ to select extraordinary high fluxes. These fluxes are clustered in time, requiring two contiguous high fluxes as a seed to start the creation of a particle burst (PB), which can be further extended if additional high fluxes are found within a moving time window. The results presented in this paper were obtained with a 5 s long window that ensured the clustering of the high fluxes observed during the GRB221009A into particle bursts while separating the main time substructures.

3.2. Geant4 Simulation of a Single HEPP-L Channel

Considering that all the HEPP-L were exhibiting high electron counts during the most intense part of the GRB, we analyzed the case where the anomalous rates were due to photon conversions in the detector structural elements. A simplified geometry of a single HEPP-L channel has been implemented in the Monte Carlo (MC) simulation toolkit GEANT4 (Agostinelli et al. 2003; v4.10.6.p01). This simulation was used to analyze the interactions of the GRB221009A photons in the HEPP-L detector. The simulated geometry includes one aluminum collimator and the sensitive silicon detectors, as well as a scintillator layer used as a anticoincidence detector. The material of the satellite and other instruments on board CSES-01 were neglected in this simulation, as it is expected that most of the low-energy electrons induced by the interaction of the GRB photons with the spacecraft material do not reach the silicon detectors and thus do not contribute significantly. Gamma rays were generated from a $30 \times 30\,cm^2$ window placed right on top of the collimator. Particles were simulated according to an isotropic flux, with $0° < \phi < 180°$ and $0° < \theta < 90°$ uniformly sampled in $\cos^2\theta$. The primary energy spectrum was sampled from a logarithmic probability distribution between 0.01 and 10 MeV. In total, 100 million photons were generated in order to ensure a significant number of particles interacting in the sensitive volume.

We selected events by requiring an energy deposition above 0.01 MeV in the thin silicon detector, above 0.1 MeV in the thick silicon layer, and no energy deposition above 0.1 MeV in the anticoincidence detector. Among the selected events, ~83% of the energy deposits originate from secondary electrons produced via photon absorption in the passive material. These secondary electrons pass through the silicon, where most of their energy is deposited. The other 17% are due to electrons directly generated in the silicon. Tests with different electromagnetic physics lists did show consistent results within 5%.

4. Observations

On 2022 October 9, at the time of GRB221009A, CSES-01 was orbiting on an N-S descending orbit passing over Central

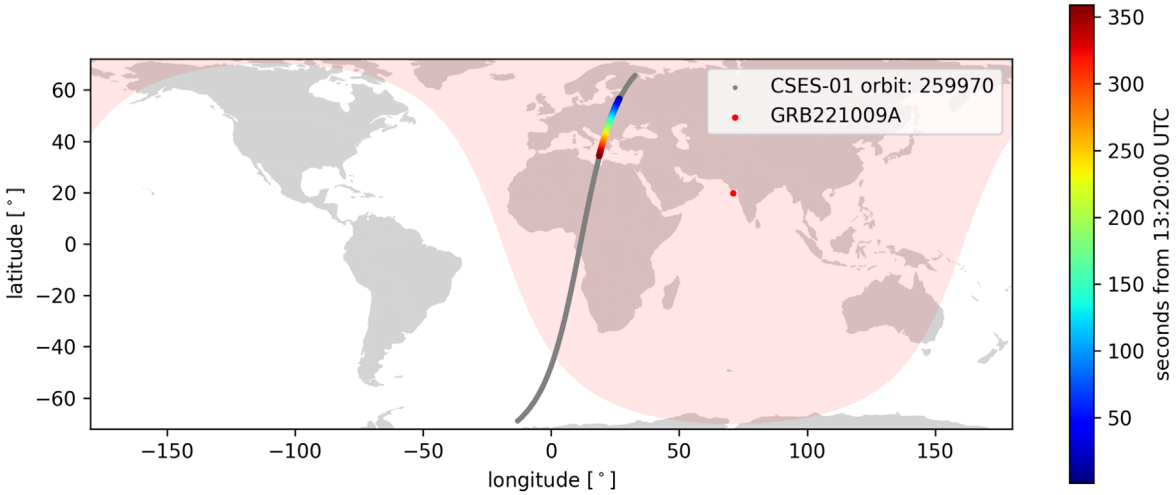

Figure 3. A map of the Earth with the CSES-01 orbit 259770 on 2022 October 9 shown in gray. The data-taking of HEPP-L started at 13:17:29 and ended at 13:54:34 UTC. The colored part along the orbit marks the seconds from 13:20:00 UTC for 6 minutes. The red shaded area shows the approximate illumination area of GRB221009A, estimated for the central impact point (red dot) at 19.°8 and 71° in latitude and longitude, respectively.

Europe well within the GRB illuminated area; see Figure 3. The satellite was far away both from the polar regions as well as from the South Atlantic Anomaly: both conditions ensure a good sensitivity to fluctuations over a small reference background.

Between 13:20 and 13:25 we observed large variations of HEPP-L electron fluxes on all the instrument channels; these fluxes were associated with a sudden jump in the measured energy spectrum, from the usual situation with the majority of the data being below 200 keV in energy to the exceptional situation where the particle energy spectra were filling the whole instrumental sensitivity, up to 3 MeV.

We analyzed in detail the time structure of these particle bursts using the HEPP-L 1 s time resolution and integrating the energy spectrum starting from 250 keV to 3 MeV. The results are shown in Figure 4, where we added HEBS 1 s photon data integrated from 400 keV to 6 MeV and normalized to the maximum HEPP-L flux. We observe that the HEPP-L electron flux is nicely matching the details of the GRB time structure measured by HEBS, both during the most intense part of the GRB (from 13:20:40 to 13:21:40 UTC) as well as during the final peak at 13:25:30 UTC.

Using the data in Figure 4, we can describe the GRB time structure as shown in Table 1.

We also tested the significance of the observed signals over the background, estimated as described in Section 3. We did this channel by channel, since the total flux levels differ strongly due to their varying acceptance. In the following we focus on channel 0, which is the one pointing closer to the zenith direction and is the least impacted by the high electron fluxes of the inner radiation belts. The flux of channel 0 is shown in Figure 5(a) for two representative energy bins lasting for 3 minutes after 13:20:00 UTC. The horizontal lines correspond to the $\mu + 3\sigma$ threshold resulting from the background estimation for the $L/\alpha_{\rm eq}$ cell for $2 \leqslant L < 3$ and $160^\circ \leqslant \alpha_{\rm eq} < 180^\circ$. The first peak shows flux values well above the threshold in all 11 energy bins. The second peak is slightly lower and crosses the threshold for 8 out of 11 energy bins. The resulting PBs, after the removal of the background and clustering, are shown in Figure 5(b) in terms of significance level. The first peak is observed to reach significances between 70σ and 150σ over all energy bins. The shaded areas mark the fluxes that belong to the same PB. Overall, the PBs of the first peak are found to have an average duration of 11.5 s, ranging from 4 to 20 s depending on the energy. The second peak is on average 6.9 s long, spanning a range from 5 to 9 s over the different energy bins. The third peak lies out of the range of the figures shown here, because its fluxes are not significant enough to pass the 3σ threshold for more than one second, and thus is not triggering the formation of a cluster or a PB.

In order to evaluate the significance of the observed PB, we tested the frequency of similar PBs over a longer time span. Figure 6(a) shows the number of energy bins that are found to contain a PB measured by HEPP-L, for each minute of available data in 2022 (January 1–October 16). The PBs are required to be found at L-shell values below 2.7, in order to exclude PBs originating from fluctuations of the radiation belts, and to span a minimum of 3 s, to reject inaccuracies of the instrument. Overall, we have found three occurrences of PBs that are found over eight different energy bins; one corresponding to the second peak of the GRB signal, and the other two are found to be residuals of radiation belt fluctuations. The filling of all energy bins for the first peak of the GRB221009A signal is a unique event in 2022. The frequency with which multiple energy bins show a PB is shown in Figure 6(b) and can be interpreted as a probability density function. Thus the probability of such an event to occur due to a statistical fluctuation can be approximated to be lower than 10^{-7}. This manifests in a clear separation of the PBs filling all 11 energy bins and underlines the outstanding nature of the signal induced by the GRB.

5. Conclusion

We investigated the source of the HEPP-L anomalous flux and we found that these fluxes match perfectly the GRB time history. A simple MC simulation describing a single HEPP-L channel (Li et al. 2019) supports the interpretation that penetrating, high-energy gamma rays produced by the GRB interact in the detector structure in the vicinity of the silicon sensors, producing prompt electrons that partially release their energy in the sensors. The perfect agreement of the time

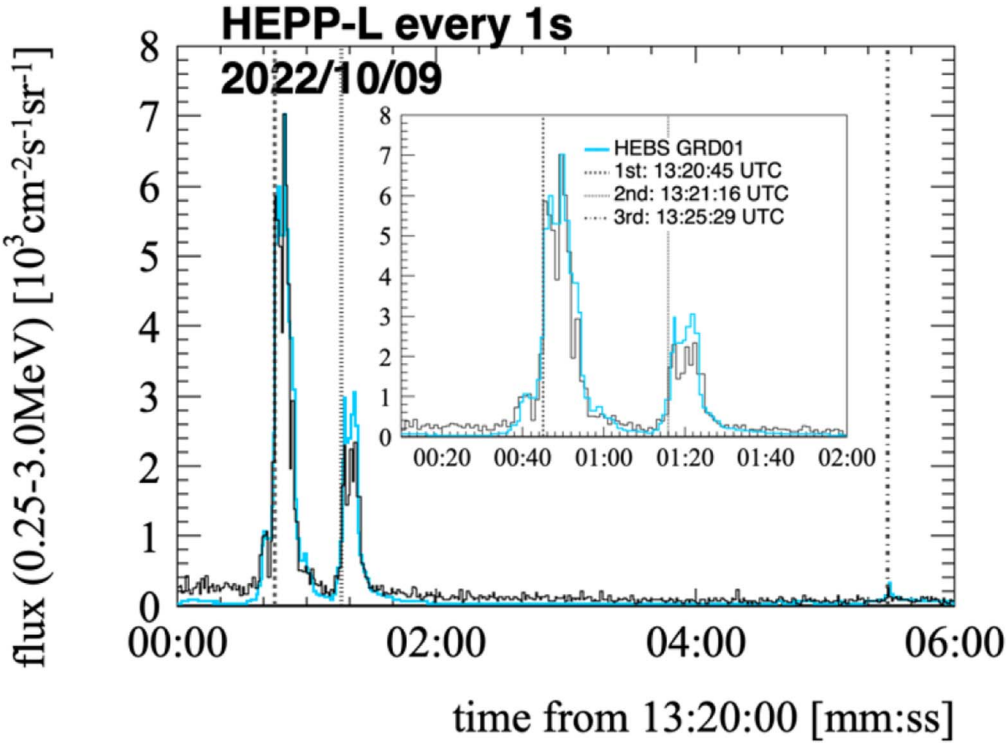

Figure 4. Electron flux of all HEPP-L channels summed over the energy range from 250 keV to 3 MeV on 2022 October 9 starting from 13:20:00 UTC. The blue curve shows the measured photon counts per second of the HEBS GRD01 instrument (Liu et al. 2022b), scaled to match the maximum of the first HEPP-L peak. The scaling factor is given in the legend. The vertical dashed lines mark the reference UTC times of the signals measured by other instruments; see Table 1. No corrections were applied to the timing provided by HEBS and HEPP-L instruments.

Table 1
GRB221009A Time Profile According to HEBS and HEPP-L Data, with 1 s Time Integration

Feature	Time Since T0 in s	Comment
Initial trigger	0 s (13:16:59 UTC)	HEBS/HEPP-L data not available
Shoulder	+219 s (13:20:38 UTC)	Beginning of first main peak
First peak	+225 s (13:20:45 UTC)	Split into at least three subpeaks
Second peak	+257 s (13:21:16 UTC)	Split into at least two subpeaks
Third peak	+509 s (13:25:29 UTC)	Final GRB peak

structure of these counting rates with the GRB time structure excludes that these signals could be due to electrons diffusing through the Earth magnetic field and reaching the detector: the diffuse flux time structure could not match subsecond GRB luminosity variations observed by HEBS, as we see from the data. We also searched for a similar behavior in other satellites equipped with low-energy charged particle detectors, namely NOAA-POES (15, 18, and 19) and MetOP (1 and 3). We observed that satellites that were fully or partially illuminated by GRB221009A (POES-15, MetOP-3, and partially MetOP-1) clearly show anomalous fluxes at the time of the two main

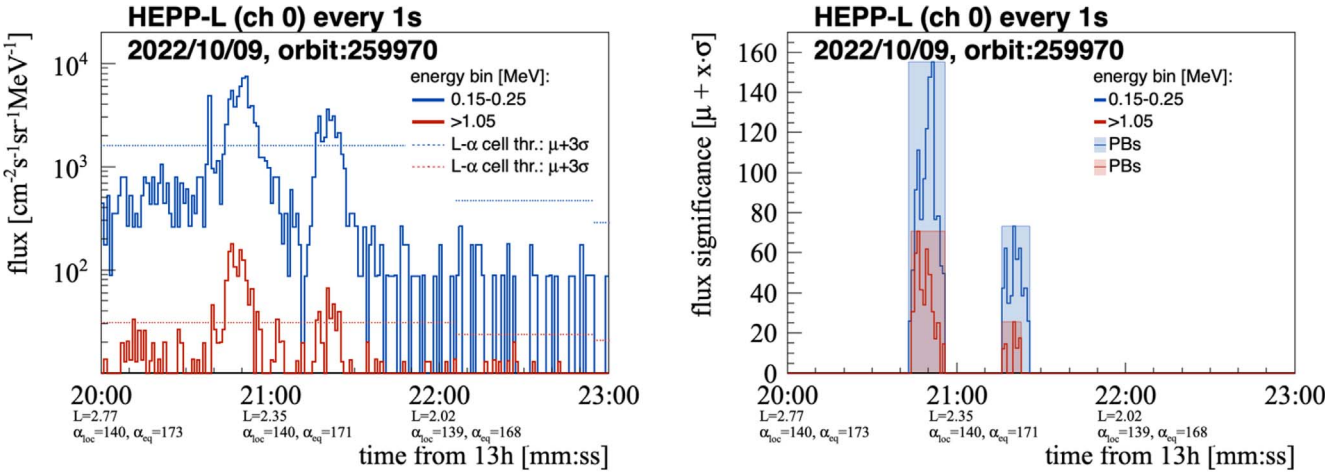

Figure 5. (a) The flux profile vs. time for channel 0 of HEPP-L. The blue and red curves show the flux corresponding to the second lowest (150–250 keV) and highest (1.05–3 MeV) energy bin, respectively. The horizontal lines mark the threshold of 3σ above the average for the corresponding L-α_{eq} bins. (b) The flux significance of the particle bursts given in the number of standard deviations above the background.

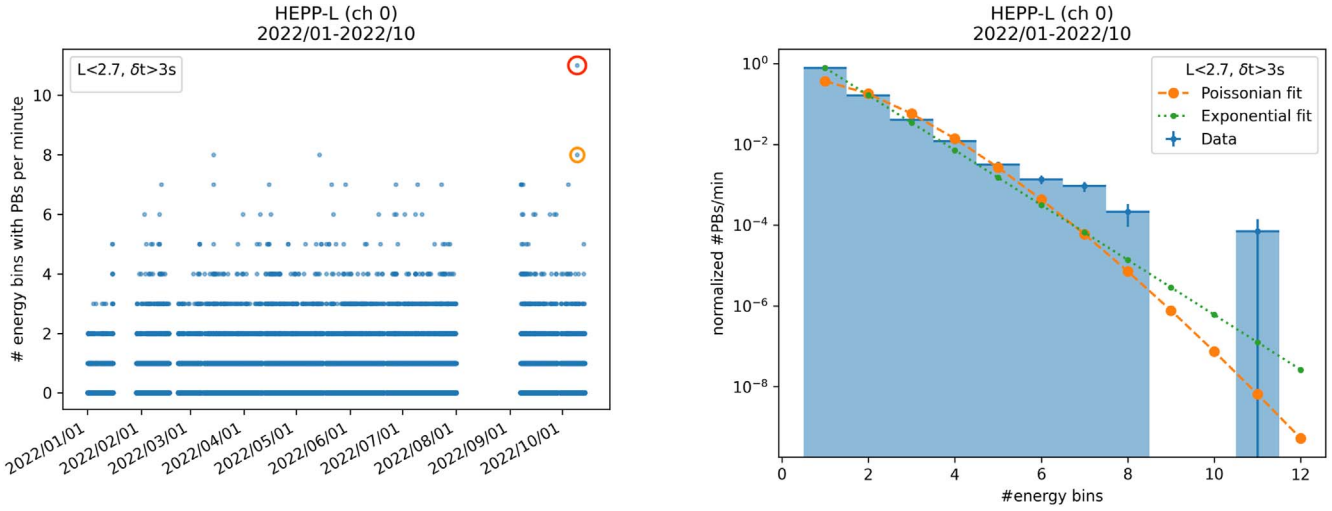

Figure 6. (a) Number of energy bins covered by PBs as a function of every minute in 2022. The PBs of the first and second peak due to the GRB221009A are circled in red and orange, respectively. The time line gaps are due to missing data, e.g., there are no data available in 2022 August. (b) Number of energy bins distribution (projection of (a) on *y*-axis) for 2022. The orange and green lines correspond to fits using a Poissonian distribution and exponential function.

GRB peaks. The analysis is currently ongoing and the results will be summarized in a future publication.

From these observation we conclude that the signal observed in HEPP-L is due to prompt production of low-energy electrons in the passive material surrounding the sensitive HEPP-L silicon detectors, providing a rate response closely matching the detailed GRB time history, providing a full solid angle coverage without any need of pointing accuracy. As the GRB221009A signal significance lays around a factor of 100 above the average electron fluxes, we plan to expand this analysis to other GRBs with the expectation to have sensitivity to GRBs that had about a factor 50 lower intensity.

The authors thank the Italian Space Agency for the financial support under the contract ASI "LIMADOU Scienza+" No. 2020-31-HH.0.

Author Contributions Statement

R.B. writing original draft, validation, review, editing and supervision; C.N. writing original draft, formal analysis, methodology, review, and editing; F.F. writing original draft, formal analysis, validation, review, and editing; R.I. review, editing, and supervision; V.V. review and editing; The remaining authors are part of the "CSES-Limadou" Collaboration whose significant contribution made satellite observations possible. All authors reviewed the manuscript and agreed to the published version of the manuscript.

Additional Information

The authors declare no competing interests.

ORCID iDs

R. Battiston https://orcid.org/0000-0002-5808-7239
C. Neubüser https://orcid.org/0000-0002-2008-8404
F. M. Follega https://orcid.org/0000-0003-2317-9560
R. Iuppa https://orcid.org/0000-0001-5038-2762
V. Vitale https://orcid.org/0000-0001-8040-7852
R. Ammendola https://orcid.org/0000-0003-4501-3289
A. Bazzano https://orcid.org/0000-0002-2017-4396
S. Beolè https://orcid.org/0000-0003-4673-8038
D. Campana https://orcid.org/0000-0003-1504-9707
M. Cristoforetti https://orcid.org/0000-0002-0127-1342
G. Gebbia https://orcid.org/0000-0001-7252-7416
M. Martucci https://orcid.org/0000-0002-3033-4824
G. Masciantonio https://orcid.org/0000-0002-8911-1561
G. Osteria https://orcid.org/0000-0002-9871-8103
E. Papini https://orcid.org/0000-0002-7969-7415
F. Palmonari https://orcid.org/0000-0003-3707-0013
A. Parmentier https://orcid.org/0000-0002-9073-3288
M. Piersanti https://orcid.org/0000-0001-5207-2944
U. Savino https://orcid.org/0000-0003-1884-2444
V. Scotti https://orcid.org/0000-0001-8868-3990
R. Sparvoli https://orcid.org/0000-0002-6314-6117
P. Ubertini https://orcid.org/0000-0003-0601-0261
V. Vilona https://orcid.org/0000-0001-9893-9419
P. Zuccon https://orcid.org/0000-0001-6132-754X

References

Agostinelli, S., et al. 2003, NIMPA, 506, 250
Ajello, M., et al. 2019, ApJ, 878, 52
Dichiara, S., Gropp, J. D., Kennea, J. A., et al. 2022, GCN, 32632, 1
Götz, D., Mereghetti, S., Savchenko, V., et al. 2022, GCN, 32660, 1
Huang, Y., Hu, S., Chen, S., et al. 2022, GCN, 32677, 1
Lesage, S., Veres, P., Roberts, O. J., et al. 2022, GCN, 32642, 1
Li, X. Q., Xu, Y. B., An, Z. H., et al. 2019, RDTM, 3, 22
Liu, J. C., Zhang, Y. Q., Xiong, S. L., et al. 2022a, GCN, 32751, 1
Liu, J. C., Zhang, Y. Q., Xiong, S. L., et al. 2022b, http://twiki.ihep.ac.cn/pub/GECAM/GRBList/HEBS-GRB221009A.png
McIlwain, C. E. 1961, JGR, 66, 3681
Mereghetti, S., Götz, D., Borkowski, J., Walter, R., & Pedersen, H. 2003, A&A, 411, 291
Neubüser, C., Battiston, R., Burger, W. J., Follega, F. M., & Vitale, V. 2023, RemS, 15, 411
Shen, X., Zong, Q.-G., & Zhang, X. M. 2018, E&PP, 2, 439
Xiao, H., Krucker, S., Daniel, R., et al. 2022, GCN, 32661, 1
Zhang, Z., Li, X., & Wang, L. 2022, JGRA, 127, e30550